Using S-wave Receiver Functions to Estimate Crustal Structure beneath Ice Sheets: an Application to the Transantarctic Mountains, the Gamburtsev Mountains, and the East Antarctic Craton

Samantha Hansen[1], Jordi Julia[1], Andrew Nyblade[1], Moira Pyle[2], Douglas Wiens[2], and Sridhar Anandakrishnan[1]

[1]Department of Geosciences, The Pennsylvania State University, USA [2]Earth and Planetary Sciences, Washington University in St. Louis, USA

Abstract

For seismic stations deployed on ice sheets, determining crustal structure using P-wave receiver functions (PRFs) can be difficult since ice reverberations may mask P-to-S (Ps) conversions from the crust-mantle boundary (Moho). In this study, we assess the usefulness of S-wave receiver functions (SRFs), which are not affected by ice multiples, for investigating crustal structure beneath ice sheets by analyzing broadband seismic data recorded across the Transantarctic Mountains (TAMs) and the East Antarctic (EA) craton. Preliminary results from the Gamburtsev Antarctic Mountains Seismic Experiment (GAMSEIS) are also shown. Clear S-to-P (Sp) conversions from the Moho are obtained using standard SRF processing methods and are easier to interpret than the corresponding Ps conversion on PRFs. When the Sp-S times are modeled together with 16-20s Rayleigh wave group velocities, we obtain Moho depth estimates of ~40-45 km for the EA craton, consistent with average Precambrian crustal thickness found globally, but ~9 km thicker than previously reported estimates. A somewhat thinner crust (~35-40 km) is obtained beneath the TAMs, suggesting that crustal buoyancy is at most a minor contributor to the uplift of the mountain range in this region.

Introduction

S-wave receiver functions (SRFs) are becoming a popular technqiue to investigate seismic discontinuities within the lithosphere that cannot be well imaged using P-wave receiver functions (PRFs). For example, it is well documented that multiples from P-to-S (Ps) conversions originating at the crust-mantle boundary (Moho) on PRFs can mask Ps conversions from the lithosphere-asthenosphere boundary (LAB), making the lithospheric structure difficult to discern. On SRFs, however, S-to-P (Sp) conversions from the LAB can be more easily identified because they arrive earlier than the direct S phase while all crustal multiples arrive later.

A similar situation arises for seismic stations on ice sheets. Multiples from the Ps conversion at the ice-rock interface may interfere with the Ps conversion from the Moho, making it more difficult to use PRFs from stations on ice to determine crustal thickness as compared to stations situated on rock. In this study, we use broadband seismic data recorded across the Transantarctic Mountains (TAMs) and the East Antarctic (EA) craton to ascertain the usefulness of SRFs for imaging the Moho beneath seismic stations deployed on ice (referred to hereafter as "ice stations").

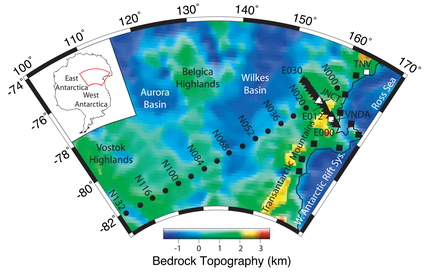

Figure 1. Map of the TAMSEIS seismic stations overlain on shaded relief bedrock topography from BEDMAP (*Lythe et al.*, 2001). Stations along the EW and NS profiles are shown by black triangles and circles, respectively, except for station JNCT (white triangle) which is common to both profiles. Other TAMSEIS stations are shown by black squares. Two stations from the Global Seismograph Network, TNV and VNDA, are also shown for reference (white squares).

Our study focuses on the east-west (EW) and north-south (NS) subarrays of the Transantarctic Mountains Seismic Experiment (TAMSEIS), which operated from December 2000 to December 2003 (Fig. 1). Since our primary goal is to evaluate SRFs for imaging the Moho beneath ice, we focused on stations located on the EA Ice Sheet: stations E012-E030 along the EW profile and stations JNCT-N132 along the NS profile (Table 1). However, to check the consistency of our results with those from previous PRF studies, we also computed SRFs for several stations deployed on rock ("rock stations") within the TAMs.

Table 1. Station coordinates and ice thicknesses

Station	Latitude (°)	Longitude (°)	Ice Thickness (km)
TAMSEIS EW Profile			
E000	-77.6262	163.6175	-
E002	-77.5750	163.0078	-
E004	-77.4133	162.0661	-
E006	-77.3703	161.6256	-
E008	-77.2817	160.5033	-
E010	-77.1853	160.0098	-
E012	-77.0461	159.3247	0.0829
E014	-76.9898	158.6217	0.7158
E018	-76.8234	157.2237	1.5252
E020	-76.7295	156.5472	1.6769
E022	-76.6280	155.9025	1.8012
E024	-76.5346	155.2500	1.4460
E026	-76.4248	154.7582	1.4861
E028	-76.3075	154.0384	2.0221
E030	-76.2510	153.3793	2.1353
TAMSEIS NS Profile			
N000	-76.0087	160.3784	-
JNCT	-76.9288	157.9012	1.1019
N020	-77.4678	155.8175	1.8991
N028	-78.0296	153.8175	2.0793
N036	-78.5508	151.2776	2.2017
N044	-79.0692	148.6159	2.2923
N052	-79.5441	145.7489	2.4111
N060	-80.0000	142.5936	2.7565
N068	-80.3911	138.9200	2.8700
N076	-80.8061	135.4326	2.5708
N084	-81.1601	131.4673	2.4454
N092	-81.4621	126.9822	2.6354
N100	-81.6910	122.4672	2.6496
N108	-81.8791	117.6036	2.5749
N116	-82.0094	112.5698	2.4109
N124	-82.0741	107.6413	2.5248
N132	-82.0751	101.9539	3.3504

S-wave Receiver Functions and Dispersion Data

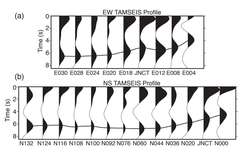
(a)
EW TAMSEIS Profile
Time (s)
E030 E028 E024 E020 E018 JNCT E012 E008 E004
(b)
NS TAMSEIS Profile
Time (s)
N132 N124 N116 N108 N100 N092 N076 N060 N044 N036 N020 JNCT N000

Figure 2. Stacked SRFs along the (a) EW and (b) NS TAMSEIS profiles. The black line denotes the Moho conversion from each station.

Stacked SRFs were generated for ice stations as well as rock stations E004, E008, and N000 for comparison to previous PRF studies. The denoted arrival (Fig. 2) observed at each stations arrives at approximately the expected time for an Sp conversion coming from the Moho. The timing of this conversion ranges between 3.9-6.6 s on the EW profile and between 4.5-6.8 s on the NS profile, where the variability of the timing indicates variations in crustal thickness or velocity.

Dispersion data for each TAMSEIS station were obtained from *Pyle et al.* (2008), who imaged the crust and upper mantle structure of the TAMs and surrounding areas using Rayleigh wave group velocities obtained from the cross-correlation of ambient seismic noise (Fig. 3).

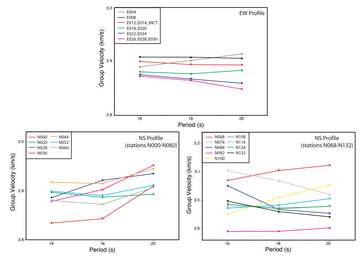

Figure 3. Smoothed Rayleigh wave group velocity dispersion curves (*Pyle et al.*, 2008). Dispersion curves for stations along the NS profile are split into two panels for clarity.

Methodology and Results

To determine if the Sp times on the SRFs (Fig. 2) can be reasonably interpreted as the Moho conversion, we model the Sp-S arrival time along with the Rayleigh wave group velocities (Fig. 3) to estimate Moho depth. A grid search procedure was used to model the data. First, synthetic dispersion curves were generated for various velocity-depth models and were compared to the observed group velocities. Then, models that fit the dispersion data within error were examined further by comparing their predicted Moho Sp time to the observed time on the corresponding stacked SRF. This gave us a range of acceptable models, such as the example shown for station E020 in Figure 4.

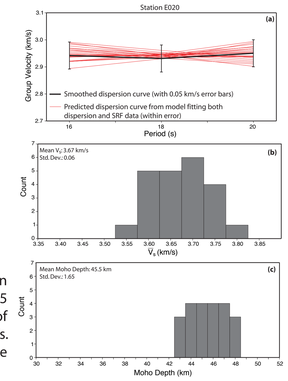

Figure 4. (a) Red lines show the predicted group velocity dispersion curves for models that fit the smoothed dispersion data within 0.05 km/s and that fit the SRF Moho Sp time within 0.3 s. (b) The range of mean crustal shear velocities (Vs) encompassed by the "fit" models. (c) The range of Moho depths encompassed by the "fit" models. Note that these Moho depths include the thickness of the ice layer.

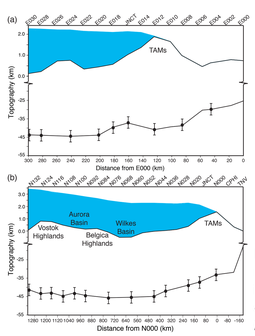

Along the EW profile, the Moho increases from ~25 km near the coast to ~40 km beneath the TAMs. There is some indication that the Moho shallows slightly beneath station JNCT; however, it then deepens beneath E018 and E020 to attain a fairly uniform depth of ~44 km beneath the end of the profile (Fig. 5a). The Vs along the profile averages ~3.6 km/s. Along the NS profile, the Moho depth also increases from the coast inland, changing from ~20 km beneath TNV to ~42 km beneath N036. Along the rest of the profile, the Moho depth across EA is fairly uniform, averaging ~44 km (Fig. 5b). Vs along this profile averages ~3.65 km/s.

Figure 5. Moho topography along the (a) EW and (b) NS TAMSEIS profiles, in relation to bedrock and surface topography. The blue shaded area indicates ice thickness and our Moho depth estimates are shown by black dots with error bars. Moho depths beneath unexamined rock stations are taken from *Finotello et al.* (2008).

Comparisons and Conclusions

Our crustal thickness estimates across the EA craton are ~9 km thicker than those reported by *Lawrence et al.* (2006), who jointly inverted PRFs and Rayleigh wave phase velocities. Predicted Moho Ps-P arrival times were computed using both our models and the models from *Lawrence et al.* (2006). For most stations, there is generally good agreement between the predicted and observed Ps arrival times (Fig. 6), illustrating the consistency between the PRFs and SRFs.

However, as shown on Figure 6, the *Lawrence et al.* (2006) predicted times are generally too early, especially for the ice stations, and do not match the observed Ps arrivals well. Therefore, the discrepancy in crustal thickness estimates between the two studies is likely related to differences in velocity.

Figure 6. Stacked PRFs along the EW TAMSEIS profile. White circles denote peaks interpreted as the Moho Ps conversion by *Lawrence et al.* (2006). The red line denotes the predicted Moho Ps-P arrival time determined using the crustal thickness and velocity estimates from our analysis (red shaded area indicates the associated uncertainty). The blue line denotes the predicted Moho Ps-P arrival time determined using the models from *Lawrence et al.* (2006).

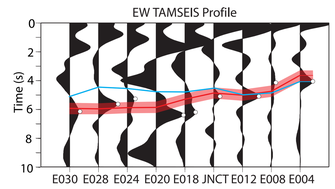

Lawrence et al. (2006) also indicated that the crust beneath the TAMs could be ~5 km thicker than beneath EA and that the thicker root may provide a source of buoyancy for the mountain range. Our results indicate that the TAMs are at most underlain by a small root that is locally thicker than the surrounding regions but is thin relative to most of the EA craton (Fig. 5). Therefore, our findings are more consistent with flexure models, in which the TAMs uplift was driven by thermal loading and erosion. Seismic tomography and gravity data also suggest similar lithospheric structure beneath EA and the TAMs, corroborating flexurally driven uplift models for this region of the mountain range.

Current Investigations: The Gamburtsev Antarctic Mountains Seismic Experiment

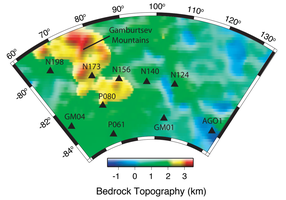

Figure 7. Map of the GAMSEIS seismic stations overlain on shaded relief bedrock topography from BEDMAP (*Lythe et al.*, 2001).

A similar approach to that taken with the TAMSEIS data is also being used to investigate the crustal structure beneath the Gamburtsev Mountains in East Antarctica. The goals of the Gamburtsev Antarctic Mountains Seismic Experiment (GAMSEIS, Fig. 7) are to (1) investigate the mechanism driving uplift of the mountains and (2) determine what role the mountains played in the formation of the EA ice sheet. Currently, data is available from ten stations, which operated between December 2007 and December 2008. Additional data is being retrieved from the field this season.

Preliminary results from GAMSEIS look promising. One station, N124, is common to both TAMSEIS and GAMSEIS. Both studies lead to comparable crustal structure beneath this station, providing additional confidence in our findings (Table 2).

Table 2. Comparison of results from station N124 from each study.

	Mean Vs (km/s)	St. Dev.	Mean Moho (km)	St.Dev.
TAMSEIS	3.68	0.08	43.4	1.65
GAMSEIS	3.67	0.09	43.6	1.61

The later Sp conversion time, especially on station N173 (Fig. 8), may indicate a thick crustal root beneath the Gamburtsev Mountains. Using approximate ice thickness and crustal velocity values for this area, we estimate a crustal thickness of ~48-50 km.

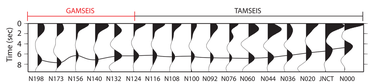

Figure 8. SRF stacks along the total NS profile, including preliminary stacks for several of the GAMSEIS stations. Again, the black line denotes the Moho conversion from each station.